

# Configuration Optimization of Supercavitating Underwater Vehicles with Maneuvering Constraints

Seong S. Ahn, Massimo Ruzzene, Francesco Scorcelletti, and Carlo L. Bottasso

S.S. Ahn and M. Ruzzene are with the School of Aerospace Engineering, Georgia Institute of Technology, 30332-0150 Atlanta GA, USA.  
F. Scorcelletti and C.L. Bottasso are with the Dipartimento di Ingegneria Aerospaziale, Politecnico di Milano, Milano 20156, Italy

# Configuration Optimization of Supercavitating Underwater Vehicles with Maneuvering Constraints

## Abstract

The paper presents configuration optimization studies on supercavitating underwater vehicles. These innovative vehicles operate at extremely high speeds due to the drag reduction achieved through the supercavitating regime. Their dynamic behavior is complex and highly nonlinear which makes their guidance and control particularly challenging. The extreme performance of the vehicles, and the complexity of their dynamic behavior drives the need for an integrated design tool that incorporates operational requirements as part of the design process.

This study is a first attempt at optimizing the configuration of supercavitating vehicles, in terms of overall dimensions, mass distributions and control surfaces size, while accounting for specific requirements related to operation at trim and during maneuvers. The optimization problem is formulated by considering range in straight level flight as the objective to be maximized, and by introducing conditions on trim operation and unsteady maneuvers as constraints. The maneuver requirements are defined by the solution of an optimal control problem, which, for a given vehicle configuration, yields optimal control inputs and corresponding vehicle state time histories.

Results are presented to demonstrate the feasibility of the process and to investigate the effect of operational constraints on the final optimal vehicle configuration. The presented methodology considers a limited spectrum of operating conditions, but it is formulated in a way that allows its extension to include a number of such operational constraints, as required by specific mission requirements.

## Index Terms

Marine vehicles, design methodology, optimization methods, optimal control.

## I. INTRODUCTION

Underwater vehicles are limited in their maximum attainable speed by the substantial drag that they produce. A new generation of weapons and vessels are being designed that use the concept of supercavitation to attain extremely high underwater speeds. In the supercavitating regime, the hydrodynamic drag is reduced compared to the classical “wetted” body case by traveling inside a self-generated bubble of water vapor. This technology offers potential important advances in underwater vehicle engineering [1], [2]. At the same time, these new vehicle concepts pose significant technical challenges in the areas of propulsion, hydrodynamics, acoustics, structural design and vehicle guidance, as well as navigation and control. Recent basic research in the area of supercavitation has led to important advances in the comprehension, modeling and simulation of hydrodynamics [1], [3], structural behavior [4], [5], and guidance and control [3], [6], [7] of supercavitating vehicles. The existing literature also identifies outstanding issues associated with the complexity of the cavity/vehicle system, the inherent instability of the vehicle, the unsteady

nature of the cavity, the complex and non-linear nature of the interactional forces between vehicle and cavity, the dynamic nature of the cavity itself, the presence of hull vibrations induced by after-body planing, surfing and tail-slapping, etc. The complexity of the problem is further increased by the need of supercavitating vehicles to be designed to maneuver aggressively and to be highly agile, in order to be able to deliver high performance while operating at the boundaries of the flight envelope. One of the major issues towards the development of a controllable, maneuvering supercavitating vehicle is associated with the fact that major questions still need to be resolved regarding the basic configuration of the vehicle itself, including its control surfaces, the control system, and the dynamic behavior of the cavity. The selection of overall vehicle dimensions, the determination of mass distributions, and the sizing of the control surfaces need to be guided by design tools that are able to optimize the vehicle configuration subjected to realistic design constraints, which integrate conditions related to the vehicle operation.

This paper represents a first step towards the development of an integrated design tool for supercavitating vehicles. The vehicle configuration, as defined by a set of parameters defining overall dimensions, and size and location of the control surfaces, as well as its nominal speed in straight and level flight, is optimized to maximize a performance index, the range in level flight in this case. The formulation of the optimization problem includes a set of design constraints, which define bounds imposed on the design variables, as well as a number of requirements related to the vehicle operation. Specifically, constraints are imposed to satisfy conditions on trimmed level and turning flight, as well as on maneuvering flight conditions. For each vehicle configuration corresponding to an iteration of the optimization problem, the maneuvering flight conditions are computed by solving constrained optimal control problems, which yield both the control inputs and the associated vehicle state time histories which minimize a user-assigned cost function while satisfying a number of user-specified operational constraints. Both trim and maneuvering flight conditions, which are found on the basis of the same high-fidelity flight mechanics model of the vehicle, implicitly enforce compatibility of the considered set of operating conditions with the complex dynamic behavior of the vehicle/cavity system. Through this approach, one derives a (range, in this case) optimal vehicle configuration, which can be trimmed in level and turning flight, and which is also able to maneuver at the boundaries of its flight envelope according to assigned criteria. To our knowledge, this is the first time that a maneuver optimal control approach is integrated in a vehicle configurational optimization to explicitly account for extreme unsteady flight conditions in the vehicle design.

The paper is organized in six sections including this introduction. Sections II and III are devoted to summaries of the tools used as engines of the optimization procedure. In particular, Section II summarizes the formulation of the flight mechanics model, which is employed both for the trim analysis and for the implementation of the trajectory optimization routine. Section III describes the trajectory optimization approach as an optimal control problem and its numerical implementation. It is important to observe that Sections II and III only provide brief descriptions, while detailed treatment of both flight mechanics and trajectory optimization formulation can be found in [8] and references therein. Section IV describes the formulation of the optimization problem, with detailed descriptions of objective function, design variables and constraints. Results of various optimization studies are presented in

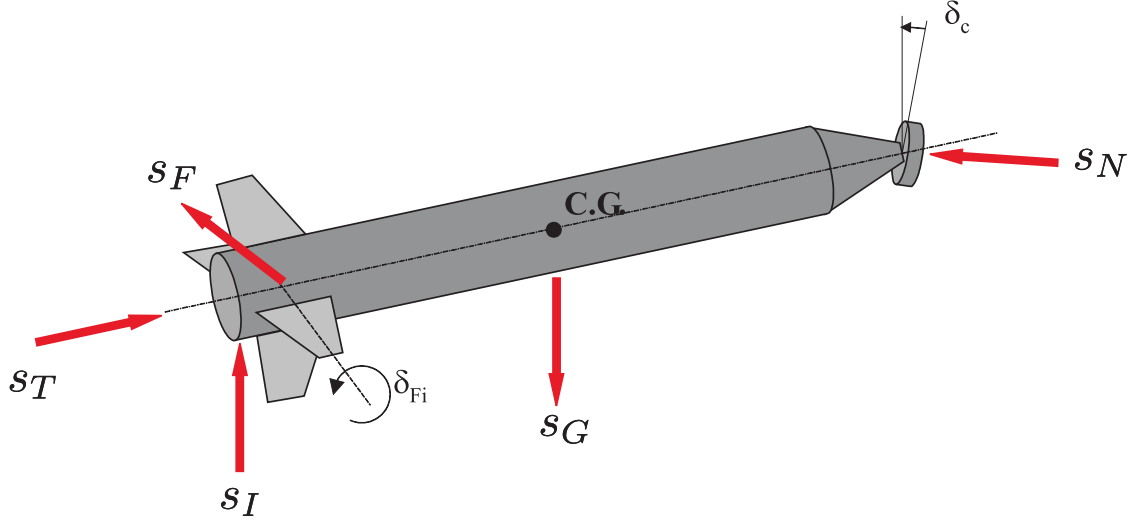


Fig. 1. Configuration of supercavitating vehicle and applied forces.

Section V, while Section VI summarizes the main findings of the work and provides recommendations for future investigations.

## II. FLIGHT MECHANICS MODEL

### A. Equations of Motion

A 6 Degree Of Freedom (DOF) rigid body model describes the dynamic behavior of the vehicle. A schematic of the vehicle configuration and of the applied forces is shown in Fig. 1. The body is acted upon by a system of forces corresponding to the interaction of the vehicle control surfaces with the cavity boundaries. The control surfaces include the fins at the back of the vehicle and the cavitator, whose primary function is the generation of the supercavity. The control surfaces provide lift, and allow for roll, pitch and yaw control. Finally, the vehicle motion is sustained by a propulsion force directed along the vehicle axis.

The equations of motion, conveniently formulated in a body-fixed reference frame  $\mathcal{B} = (\mathbf{b}_1, \mathbf{b}_2, \mathbf{b}_3)$  (see Fig. 2), are expressed as:

$$\dot{\mathbf{l}}^{\mathcal{B}} + \boldsymbol{\omega}^{\mathcal{B}} \times \mathbf{l}^{\mathcal{B}} - \mathbf{s}^{\mathcal{B}} = 0, \quad (1a)$$

$$\dot{\mathbf{h}}_P^{\mathcal{B}} + \mathbf{v}_P^{\mathcal{B}} \times \mathbf{l}^{\mathcal{B}} + \boldsymbol{\omega}^{\mathcal{B}} \times \mathbf{h}_P^{\mathcal{B}} - \mathbf{m}_P^{\mathcal{B}} = 0, \quad (1b)$$

with  $\mathbf{l} = m\mathbf{v}_P + \mathbf{S}_P^T \boldsymbol{\omega}$  denoting the linear momentum, while the angular momentum is given by  $\mathbf{h}_P = \mathbf{S}_P \mathbf{v}_P + \mathbf{J}_P \boldsymbol{\omega}$ . Letting  $\rho_V$  be the vehicle density,  $m = \int_V \rho_V dV$  is the mass of the vehicle,  $\mathbf{S}_P = \int_V \rho_V \mathbf{r} \times dV$  is the first moment of inertia,  $\mathbf{J}_P = - \int_V \rho_V \mathbf{r} \times \mathbf{r} \times dV$  is the inertia dyadic,  $\mathbf{v}_P$  and  $\boldsymbol{\omega}$  denote the linear velocity of point  $P$  and the angular velocity of the body, respectively, while  $\mathbf{s}$  and  $\mathbf{m}_P$  are the resultants of the applied forces and moments. Here and in the following, the notation  $(\cdot)^{\mathcal{A}}$  denotes components in the generic  $\mathcal{A}$  triad. If  $\mathbf{R}$  is the rotation tensor

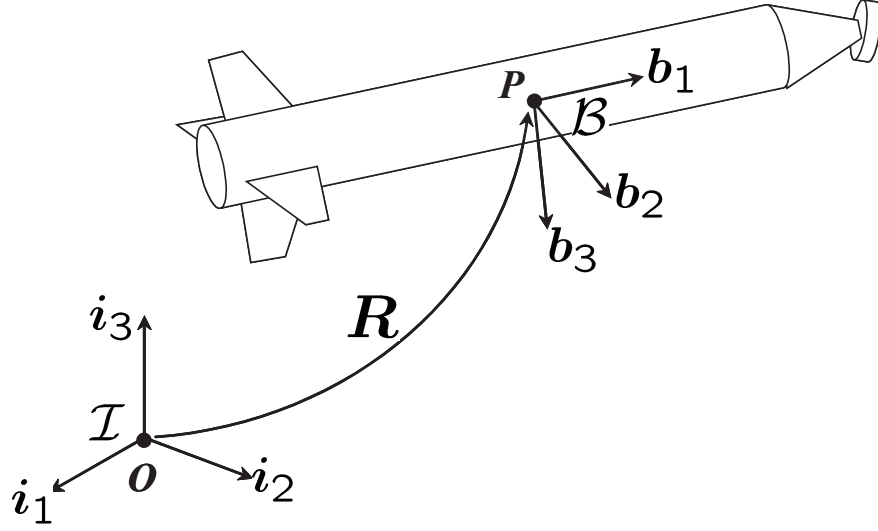


Fig. 2. Body-fixed and inertial frames.

that brings triad  $\mathcal{E}$  into triad  $\mathcal{B}$ , then the components of a generic vector  $\mathbf{a}$  in the two triads are related as  $\mathbf{a}^{\mathcal{E}} = \mathbf{R}\mathbf{a}^{\mathcal{B}}$ . Finally, the symbol  $(\dot{\cdot}) = d \cdot / dt$  indicates differentiation with respect to time.

### B. Applied Forces and Moments

The forces  $\mathbf{s}$  acting on the vehicle can be written as

$$\mathbf{s} = \mathbf{s}_T + \mathbf{s}_N + \sum_{i=1}^{n_F} \mathbf{s}_{F_i} + \mathbf{s}_I + \mathbf{s}_G, \quad (2)$$

where  $\mathbf{s}_T = \delta_T \mathbf{b}_1$  is the propulsive thrust,  $\mathbf{s}_N$  is the hydrodynamic force at the vehicle nose generated by the cavitator,  $\mathbf{s}_{F_i}$  are the hydrodynamic forces generated by the  $n_F$  fins,  $\mathbf{s}_I$  are the contact forces due to the interaction of the vehicle with the cavity, and finally  $\mathbf{s}_G = -mg\mathbf{i}_3$  is the gravitational force. Similarly, the moments  $\mathbf{m}_P$  can be written as

$$\mathbf{m}_P = \mathbf{r}_{PT} \times \mathbf{s}_T + \mathbf{r}_{PN} \times \mathbf{s}_N + \sum_{i=1}^{n_F} \mathbf{r}_{PF_i} \times \mathbf{s}_{F_i} + \mathbf{r}_{PI} \times \mathbf{s}_I + \mathbf{r}_{PG} \times \mathbf{s}_G + \sum_{i=1}^{n_F} \mathbf{m}_{F_i} + \mathbf{m}_I, \quad (3)$$

where  $\mathbf{r}_{AB}$  indicates a distance vector from point  $A$  to point  $B$ ,  $T$  is the point of application of the thrust,  $N$  is the cavitator location,  $F_i$  is the aerodynamic center of the  $i$ th fin,  $I$  is the tail-cavity contact point and  $G$  is the center of gravity. The hydrodynamic forces at the nose and at the fins depend on the motion of the vehicle, and upon shape, size and orientation of the cavity with respect to the vehicle.

The fins are controlled to provide lift in the after-body section and to maneuver the vehicle. Each fin interacts with the surrounding fluid with forces that depend on the immersion depth in the fluid, the velocity at the fin location with respect to the fluid, the fin geometry and the angle of attack. The  $i$ th fin force and moment in a local

fin-fixed reference system  $\mathcal{F}_i$  ( $i = 1, \dots, 4$ ), with origin on  $F_i$ , can be expressed as:

$$\mathbf{s}_{F_i}^{\mathcal{F}_i} = \frac{1}{2} \rho_w v_{F_i}^2 S_{\text{fin}}^2 (C_x(\gamma_{F_i}, d_{F_i}), C_y(\gamma_{F_i}, d_{F_i}), C_z(\gamma_{F_i}, d_{F_i}))^T, \quad (4a)$$

$$\mathbf{m}_{F_i}^{\mathcal{F}_i} = \frac{1}{2} \rho_w v_{F_i}^2 S_{\text{fin}}^3 (C_{mx}(\gamma_{F_i}, d_{F_i}), C_{my}(\gamma_{F_i}, d_{F_i}), C_{mz}(\gamma_{F_i}, d_{F_i}))^T, \quad (4b)$$

where  $v_{F_i}$  is the magnitude of the velocity vector at the fin frame origin  $F_i$ ,  $S_{\text{fin}}$  is the fin span length and  $C_x, C_y, C_z, C_{mx}, C_{my}, C_{mz}$  are coefficients found in [7], as obtained from detailed hydrodynamic simulations.

The hydrodynamic force acting on a circular cavitator can be expressed in a reference frame  $\mathcal{F}_N$  with origin at the cavitator center  $N$ :

$$\mathbf{s}_N^{\mathcal{F}_N} = (-L_N \sin \alpha_N - D_N \cos \alpha_N, 0, L_N \cos \alpha_N - D_N \sin \alpha_N)^T, \quad (5)$$

where  $L_N$  and  $D_N$  are respectively the lift and drag components of the hydrodynamic force, computed as [9]

$$L_N = \frac{1}{2} \rho_w v_N^2 A_N C_d(\sigma, 0) \sin \alpha_N \cos \alpha_N, \quad (6a)$$

$$D_N = \frac{1}{2} \rho_w v_N^2 A_N C_d(\sigma, 0) \cos^2 \alpha_N, \quad (6b)$$

where  $A_N$  is the cavitator area,  $v_N$  denotes the magnitude of the cavitator velocity,  $\rho_w$  is the density of the fluid, and  $\alpha_N$  is the angle of attack. Also in (6),  $C_d(\sigma, 0)$  is the cavitator drag coefficient at zero angle of attack, which is given by:

$$C_d(\sigma, 0) = C_{do}(1 + \sigma). \quad (7)$$

The cavitation number  $\sigma$  is defined as:

$$\sigma = \frac{(p_\infty - p_c)}{\frac{1}{2} \rho_w v_N^2}, \quad p_\infty = \rho_w g h + p_{\text{atm}}, \quad (8)$$

where  $p_\infty$  and  $p_c$  are the ambient fluid pressure and cavity vapor pressure,  $g$ ,  $h$ , and  $p_{\text{atm}}$  are respectively the gravity acceleration, the underwater depth, and the atmospheric pressure on the water surface. The drag coefficient at zero angle of attack and cavitation number,  $C_{do}$ , is chosen to be 0.815 according to the empirical formulation presented in [10].

Finally, during operation, the vehicle may be in contact with the internal surface of the cavity. The corresponding planing interaction is described through a model described in [11]. The model considers a planing slender body in steady forward motion on an undisturbed free surface under the assumptions of small ratio of immersion depth to body radius and large Froude numbers. Assuming a small wetted portion of a cylindrical afterbody planing on a cylindrical free surface, the planing normal and drag forces and corresponding moments can be expressed as [7],

[11] (see Fig. 3):

$$\mathbf{s}_p^B = -\pi\rho_w r_c^2 V^2 \sin\alpha_p \cos\alpha_p \left(\frac{r+h_p}{r+2h_p}\right) \left(1 - \left(\frac{\Delta}{\Delta+h_p}\right)^2\right) \mathbf{n}_3, \quad (9a)$$

$$\mathbf{m}_p^B = \pi\rho_w r_c^2 V^2 \cos^2\alpha_p \left(\frac{r+h_p}{r+2h_p}\right) \left(\frac{h_p^2}{\Delta+h_p}\right) \mathbf{n}_2, \quad (9b)$$

$$\begin{aligned} \mathbf{s}_{pf}^B = & -\frac{1}{2}\rho_w V^2 \cos^2\alpha_p C_{dp} \left(4r\frac{\Delta}{\tan(\alpha_p)} \left((1+u_c^2)\tan^{-1}(u_c) - u_c\right) \right. \\ & \left. + \frac{r^3}{2\Delta\tan(\alpha_p)} \left(\left(u_s^2 - \frac{1}{2}\right)\sin^{-1}(u_s) + \frac{1}{2}u_s\sqrt{1-u_s^2}\right)\right) \mathbf{n}_1, \end{aligned} \quad (9c)$$

$$\begin{aligned} \mathbf{m}_{pf}^B = & \frac{1}{2}\rho_w V^2 \cos^2\alpha_p C_{dp} \left(8\frac{\Delta}{h_p}\tan^{-1}\left(\sqrt{\frac{h_p}{\Delta}}\right)(r^2+2r\Delta+2\Delta^2) \right. \\ & \left. + \frac{8}{3}(2\Delta+r)\sqrt{\Delta h_p} - 8\sqrt{\frac{\Delta}{h_p}}(r^2+2\Delta^2) - 16r\sqrt{\Delta}\frac{\Delta}{h_p}\right) l_p \mathbf{n}_2, \end{aligned} \quad (9d)$$

where  $\Delta = r_c - r$  is the difference between the cavity radius  $r_c$  and body radius  $r$ , with  $u_c = \sqrt{h_p/\Delta}$  and  $u_s = (2/r)\sqrt{\Delta h_p}$ . The drag coefficient  $C_{dp}$  for a fully turbulent flow as assumed in [11] is calculated as  $C_{dp} = 0.031/(Re)^{1/7}$  [12], where  $Re$  is the Reynolds number based on the wetted longitudinal length. Accordingly, the cavity vehicle interaction force,  $\mathbf{s}_I$  in (2) is given by  $\mathbf{s}_I = \mathbf{s}_p + \mathbf{s}_{pf}$ , while the corresponding moments can be added to the moment equation (3).

### C. Cavity Model

The behavior of the cavity affects the forces at the nose of the vehicle, the immersion of the fins in the fluid, and the contact forces between vehicle and cavity boundary. While supercavitation may in general be accurately estimated by approaches based on slender-body theory, boundary element methods, and sophisticated computational methods, the following simplified models are however considered to be efficient and accurate enough to reproduce the overall dynamic behavior of a supercavitating vehicle as required by the optimization studies performed in this work. The description of the shape of the cavity is based on a model formulated according to Logvinovich independence principle [13]. The model assumes that, in the absence of viscous effects, each cavity section expands independently of adjacent sections, as a result of balance between fluid inertia and pressure difference between the cavity and the ambient liquid. The cavity radius  $r_c$  and radial expansion rate  $\dot{r}_c$  are defined as:

$$r_c = r_{\max} \sqrt{1 - \left(1 - \frac{r_o^2}{r_{\max}^2}\right) \left|1 - \frac{t}{t_{\max}}\right|^{2/\kappa}}, \quad (10a)$$

$$\dot{r}_c = \frac{r_{\max}^2}{r_c} \frac{1}{\kappa t_{\max}} \left(1 - \frac{r_o^2}{r_{\max}^2}\right) \left(1 - \frac{t}{t_{\max}}\right) \left|1 - \frac{t}{t_{\max}}\right|^{2(1-\kappa)/\kappa}, \quad (10b)$$

where  $r_o$  is the initial cavity radius,  $r_{\max} = r_N \sqrt{C_d(\sigma, 0)/\sigma}$ , is the maximum cavity radius, with  $d_c$  denoting the cavitator diameter, and  $t_{\max}$  is the time required for the cavity to achieve its maximum radius. Also, in (10)  $\kappa = 0.85$  is a correction factor based on a selected value  $C_{do} = 0.82$ , while the initial cavity radius is empirically set as  $r_o = 1.92 d_c/2$  according to [13].

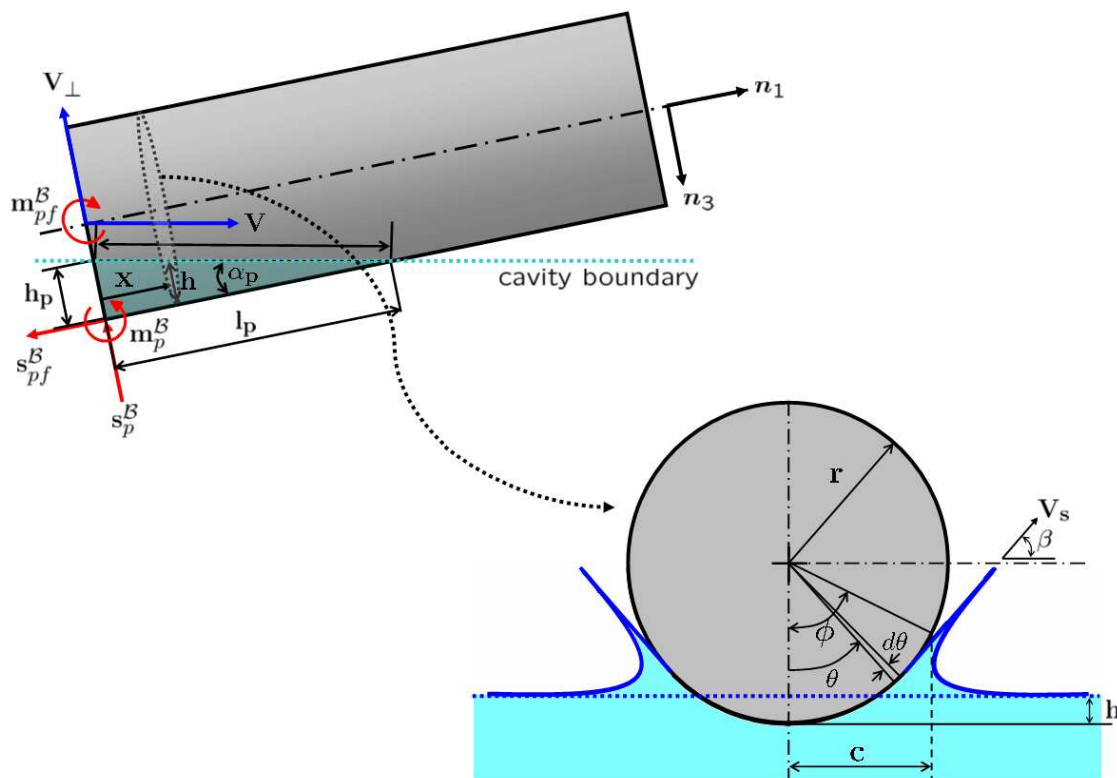


Fig. 3. Configuration of planing vehicle and wetted cross section.

### III. TRAJECTORY OPTIMIZATION TECHNIQUE

The trajectory optimization code computes maneuvers for supercavitating vehicles based on a set of requirements. Computing a maneuver means determining the time histories of the control inputs and the associated time histories of the vehicle states. Any computed maneuver must always satisfy a certain number of requirements. Maneuvers must be first compatible with the vehicle dynamics, i.e. they must satisfy the equations of motion within the admissible limits imposed by the vehicle flight envelope and the necessarily limited control authority of the vehicle actuators. Moreover, maneuvers should minimize some cost function, such as the time necessary to accomplish a given goal, or maximize the final vehicle velocity, or yet again the control effort necessary to steer the vehicle. In fact, optimality provides a way to select one meaningful solution among the typically infinite possible different ways of achieving a same goal. Finally, maneuvers must satisfy operational constraints imposed by the vehicle user.

#### A. The Maneuver Optimal Control Problem

All the above mentioned requirements can be met by expressing each maneuver as the solution of an appropriate Maneuver Optimal Control Problem (MOCP) [8], [14]. The problem time domain is here noted  $\Omega = (0, T)$ , with boundary  $\Gamma = \{0, T\}$ , where the final time  $T$  is possibly unknown. The dynamic equations of a rigid supercavitating

vehicle (see (1)) are for convenience rewritten in compact form as

$$\mathbf{f}(\dot{\mathbf{y}}, \mathbf{y}, \mathbf{u}) = 0, \quad (11)$$

The optimal control policy  $\mathbf{u}_{\text{opt}}(t)$  and associated vehicle state time histories  $\mathbf{y}_{\text{opt}}(t)$  define an optimal maneuver and minimize the cost function

$$J^{\text{mocp}} = l(\mathbf{y}, \mathbf{u}, t)|_T + \int_{\Omega} L(\mathbf{y}, \mathbf{u}, t) dt. \quad (12)$$

As previously stated, the optimal solution must satisfy the vehicle equations of motion (11), which can therefore be interpreted as constraints of the optimization problem. Constraints on the states and the controls further characterize and define the maneuver, for example by providing initial and final conditions, or by providing operational and flight envelope limits. For generality, all these conditions can be expressed as inequality constraints in the form  $x \in [x_{\min}, x_{\max}]$ , i.e.  $x_{\min} \leq x \leq x_{\max}$ . Equality constraints are enforced by simply selecting  $x_{\min} = x_{\max}$ . The initial and terminal state conditions can be written as:

$$\boldsymbol{\psi}(\mathbf{y}(0)) \in [\boldsymbol{\psi}_{0_{\min}}, \boldsymbol{\psi}_{0_{\max}}], \quad (13a)$$

$$\boldsymbol{\psi}(\mathbf{y}(T)) \in [\boldsymbol{\psi}_{T_{\min}}, \boldsymbol{\psi}_{T_{\max}}], \quad (13b)$$

while non-linear constraints on states and controls can be expressed in general as:

$$\mathbf{g}(\mathbf{y}, \mathbf{u}, t) \in [\mathbf{g}_{\min}, \mathbf{g}_{\max}]; \quad (14)$$

similarly, constraints at a (possibly unknown) internal event  $T_i$  are:

$$\mathbf{g}(\mathbf{y}, \mathbf{u}, T_i) \in [\mathbf{g}_{T_i_{\min}}, \mathbf{g}_{T_i_{\max}}]; \quad (15)$$

integral conditions on states and controls can be given as:

$$\int_{\Omega} \mathbf{h}(\mathbf{y}, \mathbf{u}, t) dt \in [\mathbf{h}_{\min}, \mathbf{h}_{\max}], \quad (16)$$

and finally upper and lower bounds are:

$$\mathbf{y} \in [\mathbf{y}_{\min}, \mathbf{y}_{\max}], \quad (17a)$$

$$\mathbf{u} \in [\mathbf{u}_{\min}, \mathbf{u}_{\max}]. \quad (17b)$$

According to optimal control theory, an optimal solution to this problem is determined by first defining an augmented performance index, obtained by adjoining the system governing equations (11) and constraints (13a–16) to the performance index (12) through the use of Lagrange multipliers (co-states). Next, the stationarity of the augmented index is imposed, resulting in the definition of a set of differential equations in the states, co-states and controls, together with a set of associated boundary conditions [14].

### B. Numerical Solution

This approach is however not always necessary nor convenient. In fact, one can avoid the derivation of the optimal control equations altogether [15] by discretizing the system equations (11) on a grid  $\mathcal{T}_h$  of the computational domain through some numerical discretization method. This defines a set of unknown parameters, which are represented by the discrete values of the states and controls on the computational grid. At this point, the problem cost function (12) and the boundary conditions and constraints (13a–16) are expressed in terms of the discrete parameters  $\mathbf{x}$ . This process defines a finite-dimensional Non-Linear Programming (NLP) problem which can be written as

$$\min_{\mathbf{x}} J_h^{\text{mocp}}(\mathbf{x}), \quad (18a)$$

$$\text{s.t.}: \mathbf{c}^{\text{mocp}}(\mathbf{x}) \leq 0, \quad (18b)$$

where  $J_h^{\text{mocp}}$  is the discrete counterpart of the cost  $J^{\text{mocp}}$  in (12), while  $\mathbf{c}^{\text{mocp}}$  are the optimization constraints, which include the discretized system dynamic equations, the discretized constraints and the boundary conditions. Here again, necessary conditions for a constrained optimum are obtained, similarly to the case of optimal control, by combining the objective  $J_h^{\text{mocp}}$  with the constraints through the use of Lagrange multipliers, and imposing the stationarity of the augmented cost function. The resulting large but sparse problem can be solved efficiently by sequential quadratic programming (SQP) methods [16] or interior point (IP) methods [17].

The discretized time grid is  $0 \equiv t_0 < t_1 < \dots < t_{n-1} < t_n \equiv T$ , composed of  $n$  intervals  $T^i = [t_i, t_{i+1}]$  of size  $h^i$ ,  $i = 0, \dots, n-1$ . Since  $T$  is in general unknown, time is mapped onto a fixed domain parameter  $s = t/T$ ,  $s \in [0, 1]$ . This yields the generic time step length as  $h^i = T(s_{i+1} - s_i)$ ,  $i = 0, \dots, n-1$ , which is now expressed in terms of the step length in the  $s$  space and of the unknown maneuver duration. The discretized system dynamics equations can be written on the generic interval  $T^i$  using the mid-point rule as

$$\mathbf{f}\left(\frac{\mathbf{y}_{i+1} - \mathbf{y}_i}{h^i}, \frac{\mathbf{y}_i + \mathbf{y}_{i+1}}{2}, \mathbf{u}^i\right) = 0, \quad i = 1, \dots, n-1, \quad (19)$$

where  $\mathbf{y}_i$ ,  $\mathbf{y}_{i+1}$  are the values of the states at times  $t_i$ ,  $t_{i+1}$ , respectively, and  $\mathbf{u}^i$  is the constant value of the controls within  $T^i$ . Note that, coherently with their algebraic nature, controls are treated as internal unknowns, which reflects the fact that no boundary conditions can be associated with these variables. Given the discretization of the equations expressed by (19), the NLP variables  $\mathbf{x}$  are defined as

$$\mathbf{x} = (\mathbf{y}_i^T (i = 0, \dots, n), \mathbf{u}^i^T (i = 0, \dots, n-1), T)^T, \quad (20)$$

i.e. they include the state values at the grid vertices, the control values on each grid element and, possibly, the final time. The cost function and all problem constraints and bounds, including (19), are expressed in terms of the NLP variables  $\mathbf{x}$  to yield the finite dimensional optimization problem (18).

## IV. FORMULATION OF THE CONFIGURATION OPTIMIZATION PROBLEM

The vehicle configuration is optimized by solving a Design Optimization Problem (DOP), where a design-relevant cost function is minimized by finding optimal values of configurational design variables. Mathematically,

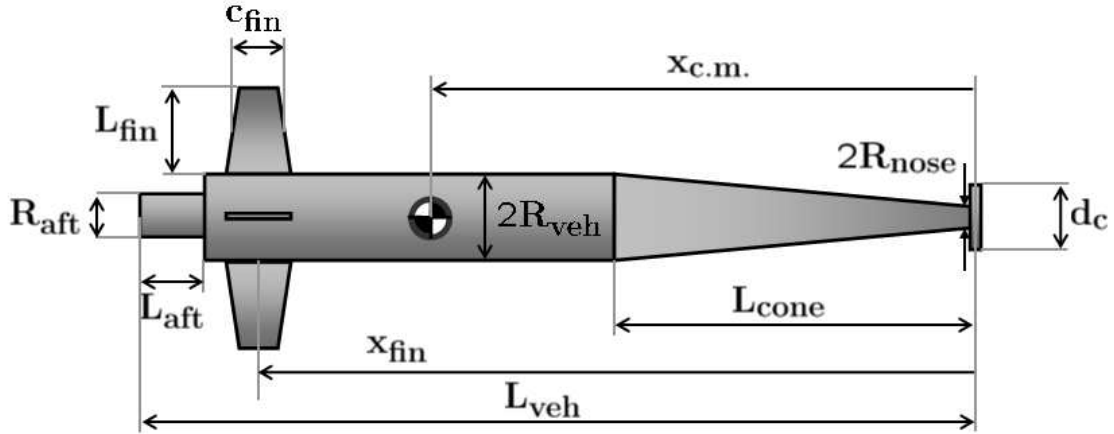


Fig. 4. Vehicle configuration.

this optimization problem is formulated as follows:

$$\min_{\mathbf{d}} J^{\text{dop}}(\mathbf{d}), \quad (21a)$$

$$\text{s.t.}: \mathbf{c}^{\text{dop}}(\mathbf{d}) \leq 0, \quad (21b)$$

where  $J^{\text{dop}}$  is the design-relevant cost function and  $\mathbf{d}$  are the design parameters. The problem is subjected to a set of equality and inequality constraints (21b), with

$$\mathbf{c}^{\text{dop}}(\mathbf{d}) = (\mathbf{c}^{\text{oper}^T}(\mathbf{d}), \mathbf{c}^{\text{conf}^T}(\mathbf{d}))^T, \quad (22)$$

where  $\mathbf{c}^{\text{oper}}$  and  $\mathbf{c}^{\text{conf}}$  respectively denote operational and configurational constraints. Both cost function and constraints depend on a number of assigned operating conditions, as described in greater detail below, which include both trimmed and maneuvering flight.

The following sections are devoted to the detailed description of design variables and objective function, and of the formulation of design and operational constraints.

#### A. Design Variables and Objective Function

The vehicle configuration used for the present study reflects projected designs for supercavitating torpedoes, according to the vehicle schematic shown in Fig. 4. The optimization process considers as a starting point a nominal vehicle whose dimensions are listed in Table I. The vector of design variables is defined as:

$$\mathbf{d} = (d_c, L_{fin}, x_{fin}, R_{veh}, L_{veh}, L_{cone}, L_{aft}, V)^T. \quad (23)$$

Notice that the design vector includes, a part from physical configurational parameters of the vehicle, also the flight speed  $V$  at trimmed level flight, which is also assumed unknown.

TABLE I  
NOMINAL VEHICLE DIMENSIONS.

Description	notation	value	unit
Vehicle mass	$m$	150	kg
Cavitator diameter	$d_c$	0.08	m
Vehicle length	$L_{veh}$	4	m
Cone length	$L_{cone}$	1.2	m
Aftertube length	$L_{aft}$	0.08	m
Vehicle radius	$R_{veh}$	0.1	m
Nose radius	$R_{nose}$	0.02	m
Aftertube radius	$R_{aft}$	0.05	m
Fin span length	$L_{fin}$	0.2	m
Fin width	$c_{fin}$	0.1	m
Fin root location	$x_{fin}$	3.87	m
Vehicle mass center location	$x_{c.m.}$	2.31	m

The travelling range during trimmed flight is the objective function to be maximized. The range can be found in several ways according to the considered flight conditions. In this study, the Breguet range equation, which is based on flight at constant velocity and lift-to-drag ratio, is used [18], [19]. If the vehicle is operating in steady level flight, then the lift-to-drag ratio is  $F_L/F_D = W/\delta_T$  from force balance considerations. Assuming constant velocity  $V$ , the range can be simply expressed as:

$$D = \int_{t_i}^{t_f} V dt = V(t_f - t_i), \quad (24)$$

where subscripts  $i$  and  $f$  respectively denote the initial and final time, and  $V$  is the trimmed velocity of the vehicle. The total flight time ( $t_f - t_i$ ) can be expressed in terms of the vehicle weight at the initial and final stages  $W_i$  and  $W_f$ , specific impulse  $I_{sp}$ , and lift-to-drag ratio  $F_L/F_D$  as:

$$t_f - t_i = I_{sp} \frac{F_L}{F_D} \ln \left( \frac{W_i}{W_f} \right). \quad (25)$$

Equation (25) is readily obtained by integrating the following relation:

$$\dot{W} = -\frac{W}{(F_L/F_D)I_{sp}}, \quad (26)$$

which is found through the rate of change of the vehicle weight  $\dot{W} = -\dot{m}_p g$ , the momentum equation of the thrust force  $\delta_T = \dot{m}_p V_{eq}$ , and the expression for the specific impulse  $I_{sp} = V_{eq}/g$ , where it is assumed that the equivalent exhaust velocity  $V_{eq}$  remains constant over time. The equivalent exhaust velocity  $V_{eq}$  accounts for the pressure difference in the engine as well as the exit velocity of the jet [20], [21]. The specific impulse  $I_{sp}$  measures the efficiency of a propulsion system, and it is defined as the total impulse exerted by the propellant divided by the

total weight of expelled propellant during engine operation [20], [21]. Equations (24) and (25) lead to the following expression for range:

$$D = V \frac{F_L}{F_D} I_{sp} \ln \left( \frac{W_i}{W_f} \right). \quad (27)$$

For simplicity, it is assumed that the mass of propellants and the weight of the warhead (payload) are proportional to the total vehicle mass. Accordingly, the range in (27) is an objective function which combines a number of configuration and performance related parameters through the following expression:

$$D = a_0 \frac{Vm}{\delta_T}, \quad (28)$$

where

$$a_0 = I_{sp} g \ln \left( \frac{1}{1 - r_{mp}} \right), \quad (29)$$

and where thrust  $\delta_T$ , vehicle mass  $m$ , and propellant-to-vehicle weight ratio  $r_{mp}$  indicate the values at the initial time. The constant  $a_0$  is an engine-specific, structure and material-related value, which is not considered to vary in terms of the set of design variables. Also, the range does not include the distances traveled before attaining trimmed velocity and after burnout. In summary, maximizing the range corresponds to minimizing the thrust force while maximizing speed and warhead weight. In the optimization problem described by (21), the objective function is therefore  $J^{\text{dop}} = -D(\mathbf{d})$  as defined by (28).

### B. Operational Constraints

The operational constraints express conditions imposed on trimmed flight and during maneuvers, and can be written as:

$$\mathbf{c}^{\text{oper}}(\mathbf{d}) = (\mathbf{c}^{\text{trim,level}^T}(\mathbf{d}), \mathbf{c}^{\text{trim,turn}^T}(\mathbf{d}), \mathbf{c}^{\text{man}^T}(\mathbf{d}))^T. \quad (30)$$

1) *Trim Constraints:* The constraints related to operation at trim are:

$$\mathbf{c}^{\text{trim,level}}(\mathbf{d}) = 0, \quad (31a)$$

$$\mathbf{c}^{\text{trim,turn}}(\mathbf{d}) = 0, \quad (31b)$$

which respectively define level flight and turning trim conditions. The generic trim constraint can be more precisely expressed as:

$$\mathbf{c}^{\text{trim}}(\mathbf{d}) = \left\{ \begin{array}{c} \boldsymbol{\omega}^{\mathcal{B}} \times \mathbf{l}^{\mathcal{B}} - \mathbf{s}^{\mathcal{B}} \\ \mathbf{v}_P^{\mathcal{B}} \times \mathbf{l}^{\mathcal{B}} + \boldsymbol{\omega}^{\mathcal{B}} \times \mathbf{h}_P^{\mathcal{B}} - \mathbf{m}_P^{\mathcal{B}} \\ \mathbf{v}^{\mathcal{B}} - \mathbf{R}_{\mathcal{B} \rightarrow \mathcal{I}}^{\mathcal{B}} \mathbf{v}^{\mathcal{I}} \\ \boldsymbol{\omega}^{\mathcal{B}} - \mathbf{R}_{\mathcal{B} \rightarrow \mathcal{I}}^{\mathcal{B}} \boldsymbol{\omega}^{\mathcal{I}} \\ \mathbf{v} \cdot \mathbf{b}_2 \end{array} \right\}, \quad (32)$$

where the first two sets of equations corresponds to Euler equations at trim,  $\mathbf{v}^{\mathcal{I}}$  and  $\boldsymbol{\omega}^{\mathcal{I}}$  in the third and fourth equation are the vehicle desired linear and angular velocity components in the inertial frame, and the last expression enforces the condition of null sideslip. The desired velocity and angular velocity inertial components define the

assigned trim conditions. For example, the velocities are assigned as  $\mathbf{v}^{\mathcal{I}} = (V, 0, 0)^T$  and  $\boldsymbol{\omega}^{\mathcal{I}} = (0, 0, 0)^T$  for level trimmed flight, while  $\mathbf{v}^{\mathcal{I}} = (V, 0, 0)^T$  and  $\boldsymbol{\omega}^{\mathcal{I}} = (0, 0, \Omega)^T$  define level turning flight conditions. Therefore, the two trim constraints define the straight and level flight condition at speed  $V$ , which we recall is among the unknown design parameters, and a trimmed turn at the same speed and at a turning rate  $\Omega$  corresponding to the maximum allowable load factor.

2) *Maneuvering Constraints: Minimum Time Optimal Maneuver:* The third constraint in (30) is here chosen as

$$c^{\text{man}} = T^{\text{mocp}}(\mathbf{d}) - T_{\text{max}} \leq 0. \quad (33)$$

This inequality expresses an upper bound condition on the time necessary to accomplish a given maneuver, specifically, a 40 deg heading change. This choice is somewhat arbitrary, and more extensive investigations of relevant flight conditions as well as maneuvers should be performed to obtain perhaps more meaningful constraints. However, this is a first attempt at introducing a maneuvering condition as part of the optimization process, and therefore a simple, somewhat relevant maneuver was considered. In future developments strategic considerations may need to be enforced, or a detailed analysis of the flight envelope and operating conditions for this class of vehicles may need to be carried out. It is however expected that such considerations could be implemented in a similar way as part of the configurational optimization.

In (33),  $T^{\text{mocp}}$  denotes the maneuvering time corresponding to the optimal heading change maneuver obtained solving the optimal control problem. This quantity clearly depends on the vehicle configuration  $\mathbf{d}$ , including the initial and final trim states corresponding to level flight at velocity  $V$ . Hence the maneuver begins and ends at trimmed states with a vehicle velocity  $V$  coincident to the one considered as an input to the level flight trim constraint, and we recall once again that  $V$  is part of the vector of unknown design variables. The maneuver constraint imposes for  $T$  to be smaller than a predefined value  $T_{\text{max}}$ . As one might expect, reducing the value of  $T_{\text{max}}$  makes the constraint more stringent, which therefore plays a larger role on the final configurational solution.

### C. Design and Cavity Related Constraints

Finally, the set of design problem constraints includes the conditions:

$$c^{\text{conf}}(\mathbf{d}) \leq 0, \quad (34)$$

which define minimum and maximum values for the design variables, and constraints imposed by the cavity dimensions for assigned state of motion.

For assigned geometry and dimensions of the vehicle, the cavity constraints strongly depend upon cavitation number ( $\sigma$ ), operating conditions ( $\mathbf{v}$ ,  $\boldsymbol{\omega}$ ), and vehicle attitude as defined by a set of rotation parameters  $\mathbf{p}$ . The constraints for level flight can be expressed as:

$$c^{\text{conf,level}} = c^{\text{conf,level}}(\sigma(V, h), \mathbf{v}(V), \mathbf{p}(\theta)), \quad (35)$$

where  $\theta$  is the pitch angle in level flight. For turning flight, the constraints can be expressed as:

$$c^{\text{conf,turn}} = c^{\text{conf,turn}}(\sigma(V, \Omega, h), \mathbf{v}(V), \boldsymbol{\omega}(\Omega), \mathbf{p}(\phi, \theta)), \quad (36)$$

where  $\phi$  is the roll angle. The cavitation number determines the cavity dimensions, which are directly related to the speed of the vehicle  $V$  and to the underwater depth  $h$  (equation (8)).

Explicit expressions of the constraints are:

$$c_1^{\text{conf}} = R_{\text{veh}} - r_c|_{\xi_1} \leq 0, \quad (37a)$$

$$c_2^{\text{conf}} = -d_{F_i} \leq 0, \quad (37b)$$

$$c_3^{\text{conf}} = -h_p|_{\xi_1} \leq 0, \quad (37c)$$

where  $\xi_1$  is a non-dimensional coordinate defining the location of the afterbody with respect to the nose. The first constraint indicates that the cavity radius must exceed the vehicle radius at the afterbody to avoid partial cavitation. The second constraint enforces the requirement that fins penetrate the cavity boundary. The third condition imposes that the immersion depth is positive in the case of planing (i.e. when the afterbody is in contact with the cavity) and negative otherwise. In the case of planing, an additional condition imposes that the immersion depth is small enough for the planing forces to be approximated by (9). This additional constraint can be approximated as:

$$c_4^{\text{conf}} = h_p|_{\xi_1} - 0.3R_{\text{veh}} \leq 0. \quad (38)$$

## V. OPTIMIZATION RESULTS

### A. Optimization in the Absence of Operational Constraints

An initial optimization study is performed by neglecting the constraints related to turning trim and maneuvering conditions. The optimization problem therefore reduces to the case of maximizing the range in straight level flight. The objective of this preliminary investigation is twofold. First, this simplified optimization problem can be used as a test of the optimization procedures and their implementation. Second, it allows exploring the design space and the corresponding variation of the selected objective function, to estimate its complexity and highlight potential convergence issues during the optimization process.

A preliminary evaluation of the complexity of the design space can be obtained by computing the objective function in terms of a reduced set of design variables. Figure 5 shows for example the range, normalized with respect to the one of the nominal vehicle, computed on a regular grid in terms of cavitator diameter  $d_c$  and vehicle velocity  $V$ . In the figure, the maximum value for the range can be clearly identified for the proper combination of the diameter  $d_c$  and speed  $V$ . The solution space appears regular, characterized by the absence of local maxima and minima, and is bounded by cavity related constraints which impose the absence of partial cavitation and fin immersion.

1) *Preliminary Optimization with a Reduced Set of Design Variables:* Based on the results presented in the previous section, a preliminary optimization is carried out for the reduced set of design variables  $V$  and  $d_c$ . Results are presented in Tables II and III, which respectively list optimal design variables, corresponding trim controls, and performance of the optimal configuration in comparison with that of the nominal vehicle design. As expected, the corresponding optimal values coincide with the maximum range shown in Fig. 5.

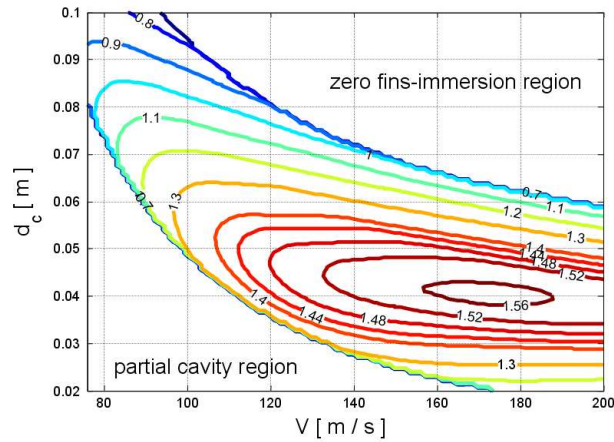


Fig. 5. Range solution space for fin-supported level flight.

TABLE II  
REDUCED OPTIMAL DESIGN CONFIGURATION.

Dimension	value	lower bound	upper bound	unit
$d_c$	0.0404	0.02	0.10	m
$V$	172.1	76	200	m/s
	controls	value	unit	
	$\delta_T$	25.8036e+3	N	
	$\delta_N$	-2.1179	degree	
	$\delta_{F_2}$	0.0765	degree	
	$\delta_{F_4}$	-0.0765	degree	
	$\delta_{F_1}$	0	degree	

TABLE III  
PERFORMANCE OF REDUCED OPTIMAL VEHICLE.

	Nominal	Optimal	unit	[%]
$D$	638.7	999.9	m	+56.5 %
$V$	78	172.0734	m/s	+120.6 %
$\delta_T$	18.3176e+3	25.8036e+3	N	+40.9 %
$m$	150	149.9452	kg	-0.04 %

2) *Optimization with a Full Set of Design Variables:* Results from the optimization with the full set of design variables are presented in Tables IV and V. Table IV shows the optimal values for the design variables in comparison

TABLE IV  
OPTIMAL DESIGN CONFIGURATION.

Dimension	value	lower bound	upper bound	unit
$d_c$	0.0400	0.04	0.11	m
$L_{\text{fin}}$	0.1500	0.15	0.25	m
$x_{\text{fin}}$	2.2975	$L_{\text{cone}}$	$L_{\text{cone}} + L_{\text{fuselage}}$	m
$R_{\text{veh}}$	0.0957	0.05	0.15	m
$L_{\text{veh}}$	4.0823	3.5	4.5	m
$L_{\text{cone}}$	0.4082	0.1 $L_{\text{veh}}$	0.9 $L_{\text{veh}}$	m
$L_{\text{aft}}$	0.0798	0.01 $L_{\text{veh}}$	0.1 $L_{\text{veh}}$	m
$m$	160.0000	140	160	kg
$V$	112.4102	76	120	m/s
	controls	value	unit	
	$\delta_T$	11.4524e+3	N	
	$\delta_N$	-4.5000	degree	
	$\delta_{F_2}$	0.2473	degree	
	$\delta_{F_4}$	-0.2473	degree	
	$\delta_{F_1}$	0	degree	

with lower and upper bounds considered in the optimization. We explicitly notice that the results of the optimization not only include configurational design parameters, but also operating conditions of the vehicle, in this case identifying the optimal nominal velocity of forward motion  $V$ . In addition, it can be observed how the mass coincides with the imposed upper bound, which may indicate the need for additional investigations where such bound is relaxed.

Table V summarizes the performance of the optimized vehicle with respect to the nominal vehicle described in section IV-A. The optimization produces a remarkable improvement in performance, which translates into a 44.1% increase in velocity, a 37.5% reduction in thrust and a combined 145.9% increase in range. The comparison between optimal and nominal vehicle configurations is shown in Fig. 6. The optimally designed vehicle is approximately of the same length of the nominal one, it has a larger volume, and most noticeably, has the set of four fins located at approximately the mid length of the vehicle. This is probably driven by imposing requirements exclusively on range in straight level flight, and the related need to reduce drag. The introduction of stability measures as part of the optimization process may significantly modify this optimal configuration. The analysis of stability of the vehicle is not addressed in the current work, as it deserves an extensive and dedicated study due to the complexity introduced by the interaction between vehicle and cavity.

TABLE V  
PERFORMANCE OF OPTIMAL VEHICLE.

	Nominal	Optimal	unit	[%]
$D$	638.7	1570.5	m	+145.9 %
$V$	78	112.4102	m/s	+44.1 %
$\delta_T$	18.3176e+3	11.4524e+3	N	-37.5 %
$m$	150	160.0	kg	+6.7 %

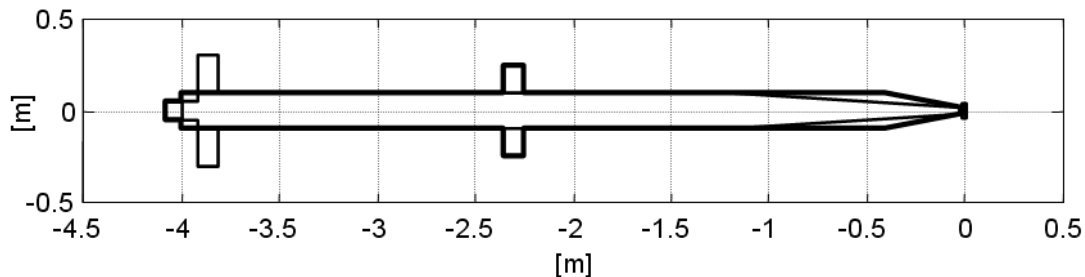


Fig. 6. Comparison between optimal (thick line) and nominal (thin line) configurations in the absence of operational constraints.

### B. Optimization with Operational Constraints

1) *Exploration of the Design Space:* The optimization results presented in the previous sections show that the range as an objective function is characterized by a regular behavior. This leads to an optimization problem which is easy to solve and does not typically suffer from the presence of local minima. The introduction of turning trim flight as a constraint does not introduce significant complexity, while the addition of the maneuvering flight condition through (33) complicates the problem. In fact, this constraint is characterized by a complex nonlinear behavior which severely affects the design space. Figure 7 shows for example the variation of the minimum flight time for the heading-change maneuver in terms of  $V$  and cavitator diameter  $d_c$ . Depending on the time bound  $T_{\max}$  selected in (22), the maneuvering constraint may produce a non-convex and/or discontinuous design space. This is illustrated in Fig. 8, which shows the outlines of the feasible design spaces corresponding to different maneuvering time bounds, and depicts with a dot the optimal solution of the unconstrained optimization over this smaller range. Selecting  $T_{\max} = 4.9$  sec for example generates a single non-convex feasible region, while imposing a smaller time such as  $T_{\max} = 4.5$  sec produces three disconnected feasible regions. It is interesting to note, that this optimal value falls outside of the feasible space when a stricter requirement is imposed on the maneuvering time. The multi-modal, non-convex structure of the design space caused by the constraints makes the optimization problem difficult in terms of global minimum evaluation and computational efficiency.

2) *A Simple Optimization Strategy:* The complexity of the design space resulting from the application of the constraints is here handled through the application of a simple optimization strategy. The approach used here is

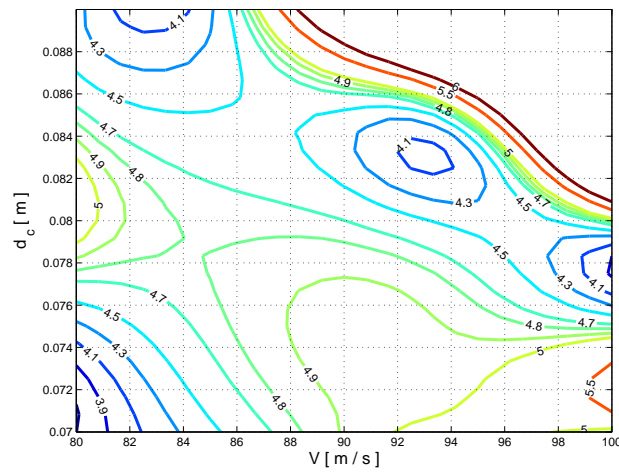


Fig. 7. Variation of the minimum flight time in terms of  $V$  and  $d_c$  for a heading-change maneuver.

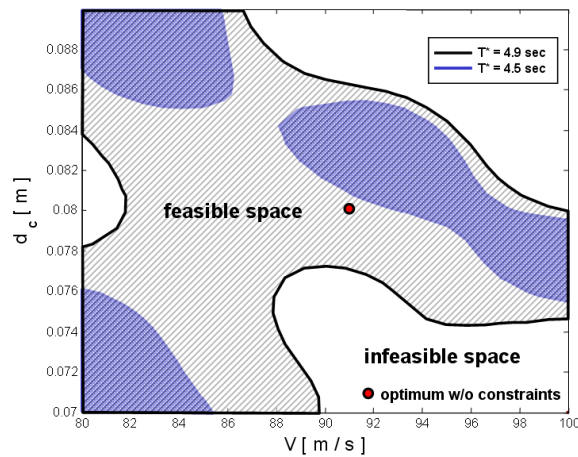


Fig. 8. Feasible design regions for different choices of maximum allowed time for the maneuver.

based on the assumption that the problem under consideration features a smooth objective function, and complex constraints. The process consists in several stages.

At the first stage, the minimum of the regular objective function is found through an unconstrained optimization, in order to avoid the solution being trapped in local feasible regions. The main idea is illustrated in Fig. 9. For example, if one considers the requirement of minimum maneuvering time as  $T_{\max} = 4.5$  sec, the initial guess may cause the solution to be trapped in a local feasible pocket (lower left corner of the figure), which is far from the optimum value corresponding to the unconstrained case.

At the second stage, constraints are evaluated at the current optimal value estimate to verify whether they are violated or not. If the optimal value estimate lies in a feasible region, then the process is considered complete. In

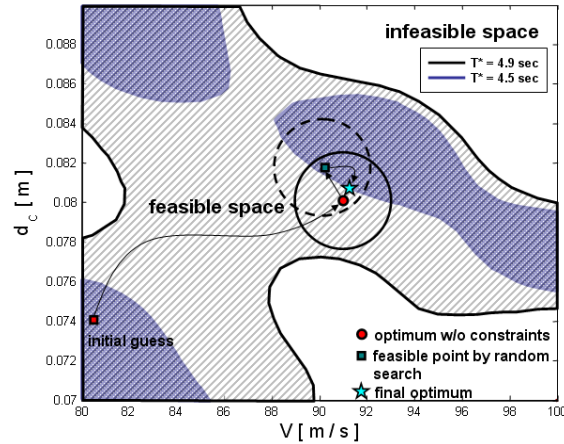


Fig. 9. Illustration of the simple optimization strategy adopted for the solution of the constrained problem.

contrast, if constraints are violated, a feasible design point is searched in a region neighboring the optimal value estimate, defined by a predetermined radius (red circle in the figure). The radius restricts the design space around the unconstrained global optimum. Once a feasible point is found through a random search, the design space is centered at this feasible point and the constrained optimization is performed in this restricted space (green circle in the figure), whose radial distance from the found feasible design point will be the same as the previous reduced region.

The radius of the reduced search space is selected on the basis of some knowledge of the design space. For example the constraints can be evaluated along the optimization path generated during the unconstrained optimization. This information can be used to evaluate the number of transitions between feasible and infeasible regions, and the percentage of feasible points out of the entire number of design points evaluated along the path line. This data can guide the selection of the search radius. As a result, this method looks for the optimum value in a feasible region close to the unconstrained optimum value. In addition, it is expected that the solution can be found with a significantly lower number of constraints evaluations.

This simple approach works well in practice when the optimization problem has the following characteristics: 1) the objective function is well-behaved and continuous over the entire design space; 2) the objective function is computationally inexpensive; 3) the constraints produce a non-convex and discontinuous feasible design space; 4) the evaluation of the constraints is computationally expensive. A more robust and efficient method may consider a more sophisticated procedure to guide the reduction of the design space and the random search, for which probabilistic and statistic information regarding the design space may be used. Tests of the developed approach on sample examples are found in [22].

3) *Preliminary Optimization with a Reduced Set of Design Variables:* A preliminary optimization with a reduced number of design variables ( $V$  and  $d_c$ ) is carried out as in Section V-A1. The influence of various constraints on

TABLE VI  
REDUCED OPTIMAL DESIGN CONFIGURATION WITH RELAXED CONSTRAINTS.

Dimension	nominal	optimal	lower bound	upper bound	unit
$d_c$	0.08	0.0404	0.02	0.10	m
$V$	78	172.0734	76	200	m/s
Constraints					
Load factor		$n$	1.1		
Maneuvering time		$T_{\max}$	40 sec		

TABLE VII  
PERFORMANCE OF REDUCED OPTIMAL VEHICLE WITH RELAXED CONSTRAINTS.

	Nominal	Optimal	unit	[%]
$D$	638.7	999.9	m	+ 56.5 %
$T$	4.9927	5.5508	sec	+ 11.2%
$V$	78	172.0734	m/s	+ 120.6 %
$\delta_T$	18.3176e+3	25.8036e+3	N	+ 40.9 %
$m$	150	149.9452	kg	- 0.04 %

maximum range is investigated by conducting several analyses with increasing requirements on turning load factor  $n$ , and on the maneuvering time bound  $T_{\max}$ .

As a first case, the optimization is carried out with all constraints being relaxed, i.e. with sufficiently low load factor and large  $T_{\max}$ . Results are presented in Tables VI and VII. As one might expect, the solution yields results which coincide with those obtained in Section V-A1 (see Table II and III). Figure 10 shows the evolution of objective function, constraints, and design variables during the optimization process. Figure 10(b) shows the operational constraints, i.e. the squared norm of the residuals of the trim equations and the bound on the optimal maneuver time  $T/T_{\max} - 1$ . Also, in case of violation of one of the constraints, the normalized values is set to 1. The plot in Fig. 10 clearly shows how during the optimization all of the constraints remain inactive, except for one instance at iteration 5. The corresponding configuration at this iteration however is such that the vehicle cannot support trim in level flight, which automatically makes both the solution for turning trim and the maneuver problem infeasible. The variation of the design variables during the optimization is shown in Fig. 10 (c), where the values are normalized with respect to their nominal values  $V_n = 85$  m/s, and  $d_{cn} = 0.08$  m. The convergence to the optimal solution is achieved after approximately 20 iterations.

A second optimization is performed with stricter constraints on load factor and minimum maneuvering time. The value of  $T_{\max}$  is set equal to 5.5 sec on the basis of the results of the previous optimization, which found that

TABLE VIII  
REDUCED OPTIMAL DESIGN CONFIGURATION WITH ACTIVE CONSTRAINTS.

Dimension	nominal	optimal	lower bound	upper bound	unit
$d_c$	0.08	0.0432	0.02	0.10	m
$V$	78	175.8683	76	200	m/s
Constraints					
Load factor		$n$	2		
Maneuvering time		$T_{\max}$	5.5 sec		

TABLE IX  
PERFORMANCE OF REDUCED OPTIMAL VEHICLE WITH ACTIVE CONSTRAINTS.

	Nominal	Optimal	unit	[%]
$D$	638.7	994.2	m	+ 55.7%
$T$	4.9927	5.4764	sec	+ 9.7%
$V$	78	175.8683	m/s	+ 125.5%
$\delta_T$	18.3176e+3	26.5258e+3	N	+ 44.8 %
$m$	150	149.9479	kg	- 0.03%

the optimal vehicle performed the specified heading change maneuver in 5.55 sec (see Table VII). Results of the optimization, bounds and constraint values are listed in Table VIII, while Table IX compares the performance of the optimal vehicle with that of the nominal one. The variations of objective, constraints and design variables during this optimization are presented in Fig. 11, which clearly shows how the constraint on the maneuvering time affects the optimization by becoming active at several instances. The resulting optimal parameters are slightly different with respect to the unconstrained one, and so is the performance of the corresponding vehicle, which shows a minor reduction in the optimal range. This simple case illustrates how the constraint on the maneuvering time may introduce conflicting requirements on the vehicle configuration with respect to those dictated by the objective function, and the need to obtain a final compromise. The minor changes in performance and optimal parameters are related to the fact that the minimum maneuvering time is chosen very close to the one resulting from the unconstrained optimization.

### C. Optimization with a Full Set of Design Variables

The final set of optimization studies considers the full set of design variables. As in the previous case, the effect of increasingly strict constraints is estimated through the solution of various problems. The first optimization considers the relaxed constraints listed in Table X, which also presents the optimal vehicle and the bounds assigned to the design variables. The performance of the optimal vehicle is summarized in Table XI. As expected, the solution of the

TABLE X  
OPTIMAL DESIGN CONFIGURATION WITH RELAXED CONSTRAINTS.

Dimension	value	lower bound	upper bound	unit
$d_c$	0.0400	0.04	0.11	m
$L_{fin}$	0.1500	0.15	0.25	m
$x_{fin}$	2.2975	$L_{cone}$	$L_{cone} + L_{fuselage}$	m
$R_{veh}$	0.0957	0.05	0.15	m
$L_{veh}$	4.0823	3.5	4.5	m
$L_{cone}$	0.4082	$0.1 L_{veh}$	$0.9 L_{veh}$	m
$L_{aft}$	0.0798	$0.01 L_{veh}$	$0.1 L_{veh}$	m
$V$	112.4102	76	120	m/s
$m$	160.0	140	160	kg
Constraints				
Load factor		$n$	1.1	
Maneuver time		$T_{max}$	40 sec	

TABLE XI  
PERFORMANCE OF OPTIMAL VEHICLE WITH RELAXED CONSTRAINTS.

	Nominal	Optimal	unit	[%]
$D$	638.7	1570.5	m	+ 145.9%
$T$	4.9927	3.8070	sec	- 23.7 %
$V$	78	112.4102	m/s	+ 44.1%
$\delta_T$	18.3176e+3	11.4524e+3	N	- 37.5 %
$m$	150	160.0	kg	+ 6.7 %

optimization with highly relaxed constraints coincides with the one obtained in Section V-A2 (see Table IV and V). It is interesting to note that, in addition to the same improvement in velocity, thrust and range, the optimal vehicle also produces a 23.7% reduction in maneuvering time. The mass of the obtained vehicle coincides with the imposed upper bound, while the size of control surfaces (fins and cavitator) coincides with the imposed lower bounds, which indicates that larger design intervals may need to be considered. The low occurrence of constraint violations during the optimization iterations, and therefore their relative inactivity throughout the process, is demonstrated by the plot in Fig. 12(a).

The results with stricter constraints are presented in Tables XII and XIII. The history of the normalized constraints presented in Fig. 12(b) shows their increased activity, and frequent violations in particular in the beginning stages of the optimization process. The performance summary confirms that the reduction in allowable maneuvering time and

TABLE XII  
OPTIMAL DESIGN CONFIGURATION WITH ACTIVE CONSTRAINTS.

Dimension	value	lower bound	upper bound	unit
$d_c$	0.0412	0.04	0.11	m
$L_{fin}$	0.1508	0.15	0.25	m
$x_{fin}$	2.4486	$L_{cone}$	$L_{cone} + L_{fuselage}$	m
$R_{veh}$	0.0943	0.05	0.15	m
$L_{veh}$	4.1244	3.5	4.5	m
$L_{cone}$	0.4370	$0.1 L_{veh}$	$0.9 L_{veh}$	m
$L_{aft}$	0.1013	$0.01 L_{veh}$	$0.1 L_{veh}$	m
$V$	112.7372	76	120	m/s
$m$	155.8	140	160	kg
Constraints				
Load factor		$n$	2	
Maneuver time		$T_{max}$	4.5 sec	

TABLE XIII  
PERFORMANCE OF OPTIMAL VEHICLE WITH ACTIVE CONSTRAINTS.

	Nominal	Optimal	unit	[%]
$D$	638.7	1512.2	m	+ 136.8 %
$T$	4.9927	4.3612	sec	- 12.6 %
$V$	78	112.7372	m/s	+ 44.5 %
$\delta_T$	18.3176e+3	11.6169e+3	N	- 37.9 %
$m$	150	155.8	kg	+ 3.9 %

the increase in load factor correspond to a reduction in the optimal range, which demonstrates that a compromise must be reached in the presence of additional requirements. The optimized configurations for loose and strict constraints, displayed schematically in Fig. 13, show relatively small differences in configuration. Again, this is associated to the fact that the minimum required time is not dramatically different from the one corresponding to the unconstrained optimal configuration.

In order to identify how the constraints are active and how these affect the final optimal solution, optimization is carried out with different requirements on the maneuvering time  $T_{max}$  and with  $n = 2$ . The results are listed in Table XIV. In all cases, the same lower and upper bounds considered in Table X are applied for velocity, design variables and vehicle weight. The results show how the primary performance is adjusted by the imposed requirements on maneuvering time. As the required maneuvering time decreases (more stringent), the performance

TABLE XIV  
PERFORMANCE OF OPTIMAL VEHICLE WITH VARIOUS CONSTRAINT LIMITATIONS

Cases	Performances				Constraints		
	$D$ (m)	$T$ (sec)	$V$ (m/s)	$\delta_T$ (N)	$m$ (kg)	$n$	$T_{\max}$ (sec)
1	1551.4	4.5596	111.8540	11.3672e+3	157.7	2	5.50
2	1512.2	4.3612	112.7372	11.6169e+3	155.8	2	4.50
3	1498.0	4.0918	112.3307	11.3822e+3	151.8	2	4.25

of the vehicle decreases. This preliminary study also shows that the constraints produce cross-coupling effects on the primary performance. For example, the history of active constraints on turn rate changes due to different optimization paths caused by the maneuvering time constraint being active. It is also important to note that the maneuver time bound  $T_{\max}$  considered in Table XIV has been chosen as the lower limit for which the optimization procedure is able to converge to a result. The range of  $T_{\max}$  for which the time constraint is active and affects the design is thus quite narrow, as it spans approximately from 4.25 to 5.5 sec. For  $T_{\max} > 5.5$  sec the constraint does not influence the design, while for  $T_{\max} < 4.25$  sec the optimization does not converge. The lack of convergence is the result of the vehicle not being able to meet the imposed requirements, which are therefore not compatible with the vehicle characteristics as considered in this work. This limitation can be overcome if drastic modifications to the vehicle configurations are considered. This procedure, therefore, can be also used to estimate the operational limits of the considered class of vehicles and to compare fundamentally different designs, which for example may feature a cavitator with a higher number of controllable degrees of freedom, thrust vectoring capabilities, and different numbers of fins. The analysis and comparison of different design solutions will need to be supported by more sophisticated optimization tools, which are more computationally efficient and more robust in the presence of local minima and disconnected design spaces. The efficiency of the optimization process may be enhanced for example through the use of response surface methods to perform local approximations of the design space. This approach is currently under investigation

## VI. CONCLUSIONS

In this work, the configuration and nominal operating speed of a supercavitating vehicle are optimized by integrating several operational requirements in the optimization process. Specifically, trim conditions in level and turning flight, as well as a heading-change maneuver are considered as constraints in a system-level optimization which seeks to maximize range during straight level flight.

The requirements on turning performance and maneuverability affect the final optimal solution when all constraints are active based on the imposed limitations. Strict requirements reduce the amount of improvement in performance as a result of their restricting the feasible design space, while the solutions with relaxed constraints approach those previously obtained during the optimization process without constraints. The presented results show how constraints

related to the considered maneuver may introduce significant complexity in the design space, and make the solution of the optimization more difficult. A simple optimization strategy is employed to handle a disconnected design space and to improve the computational efficiency of the process.

The proposed procedure may be extended to include additional operational constraints, which may be dictated by specific strategic requirements. In addition, it may be used to identify performance limitations of a given design class, and to carry out comparisons between different design configurations. This should be supported by improved optimization procedures which are more robust and computationally efficient.

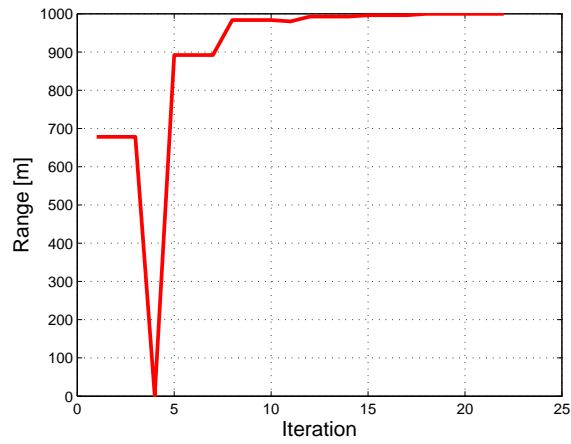
#### ACKNOWLEDGMENTS

This work is supported through a grant from the Office of Naval Research (Grant N00014-06-1-0076). The authors gratefully acknowledge the guidance and support of Dr. Kam Ng, Technical Monitor and Program Manager.

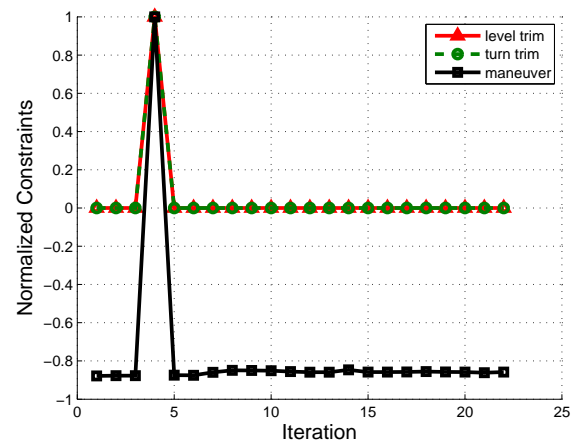
#### REFERENCES

- [1] S. Ashley, "Warp-drive underwater," *Scientific American*, May 2001.
- [2] D. Miller, "Going to war in a bubble," *International Defense Review*, December 1995.
- [3] I. N. Kirschner, N. E. Fine, J. S. Uhlman, D. C. Kring, B. J. Rosenthal, T. A. Gieseke, R. Kuklinski, A. N. Varghese, D. R. Stinebring, J. E. Dzielski, J. W. Lindau, and R. F. Kunz, "Supercavitation research and development," in *Anteon Corporation - Engineering Technology Center, Naval Undersea Warfare Center Division, Applied Research Laboratory/Penn State University*, Waikiki, HI, October 2001.
- [4] J.-Y. Choi, M. Ruzzene, and O. Bauchau, "Dynamic analysis of supercavitating vehicles using modal based elements," *Transactions of the Society for Simulation International*, vol. 80, no. 11, pp. 619–633, 2004.
- [5] M. Ruzzene and F. Soranna, "Impact dynamics of stiffened elastic supercavitating underwater vehicles," *Journal of Vibration and Control*, vol. 10, no. 2, pp. 243–267, 2004.
- [6] J. Dzielski and A. Kurdila, "A benchmark control problem for supercavitating vehicles and an initial investigation of solutions," *Journal of Vibration and Control*, vol. 9, pp. 791–804, 2003.
- [7] I. N. Kirschner, D. C. Kring, A. W. Stokes, N. E. Fine, and J. James S. Uhlman, "Control strategies for supercavitating vehicles," *Journal of Vibration and Control*, vol. 8, pp. 219–242, 2002.
- [8] R. Kamada, M. Ruzzene, F. Scorcelletti, and C. Bottasso, "Trajectory optimization strategies for supercavitating underwater vehicles," *Journal of Vibration and Control*, 2007, to appear.
- [9] T. Kiceniuk, "An experimental study of the hydrodynamic forces acting on a family of cavity producing conical bodies of revolution inclined to the flow," California Institute of Technology, Pasadena, CA, CIT Hydrodynamic Report E-12.17, 1954.
- [10] A. May, "Water entry and the cavity-running behavior of missiles," Naval Surface Weapons Center, White Oak Laboratory, Silver Spring, MD, SEAHAC Technical Report 75-2, 1975.
- [11] S. E. Hassan, "Analysis of hydrodynamic planing forces associated with cavity riding vehicles," 2004, private communication.
- [12] F. M. White, *Fluid Mechanics*, 3rd ed. New York: McGraw-Hill, 1994.
- [13] G. V. Logvinovich, "Hydrodynamics of free-boundary flow," U.S. Department of Commerce, Washington, DC, Tech. Rep., 1972, translated from the Russian( NASA-TT-F-658).
- [14] J. Arthur E. Bryson and Y.-C. Ho, *Applied Optimal Control*. New York: Hemisphere Publishing Corporation, 1975.
- [15] J. T. Betts, "Practical methods for optimal control using non-linear programming," *SIAM*, 2001.
- [16] A. Barclay, P. E. Gill, and J. B. Rosen, "Sqp methods and their application to numerical optimal control," Department of Mathematics, University of California, San Diego, CA, Report NA 97-3, 1997.
- [17] J. Renegar, "A mathematical view of interior point methods in convex optimization," *SIAM, Philadelphia*, 2001.
- [18] E. L. Fleeman, *Tactical Missile Design*, ser. AIAA Education Series. Reston, VA: American Institute of Aeronautics and Astronautics, Inc., 2001.

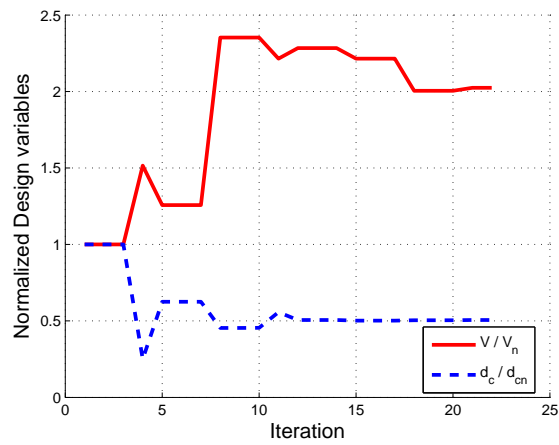
- [19] M. Asselin, *An Introduction to Aircraft Performance*, ser. AIAA Education Series. Reston, VA: American Institute of Aeronautics and Astronautics, Inc., 1997.
- [20] W. T. Thomson, *Introduction To Space Dynamics*, 2nd ed. New York: Dover Publications, INC., 1986.
- [21] P. G. Hill and C. R. Peterson, *Mechanics and Thermodynamics of Propulsion*, 2nd ed. Addison-Wesley Publishing Company, Inc., 1992.
- [22] S. S. Ahn, "An integrated approach to the design of supercavitating underwater vehicles," Ph.D. dissertation, School of Aerospace Engineering, Georgia Institute of Technology, 2007.



(a) Range

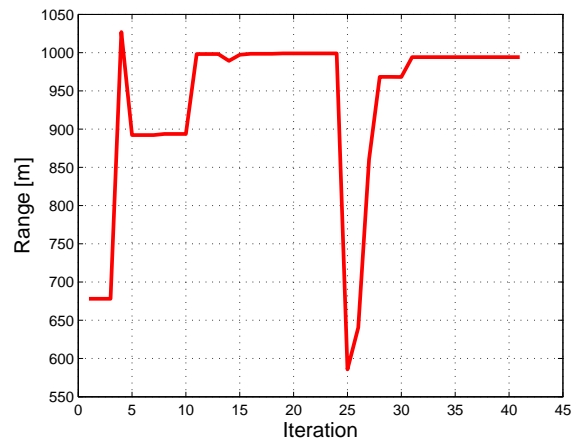


(b) Constraints

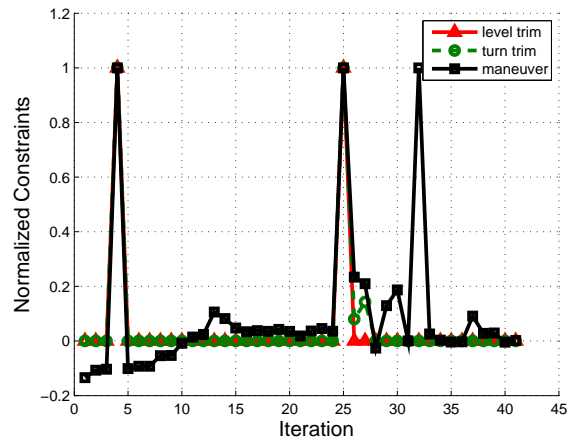


(c) Design variables

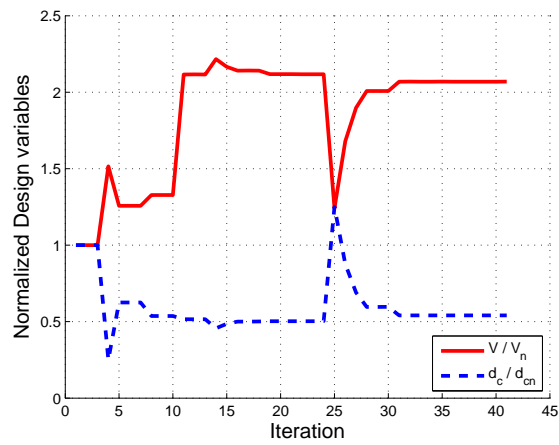
Fig. 10. Evolution of objective, constraints, and design variables during the optimization process with relaxed constraints.



(a) Range

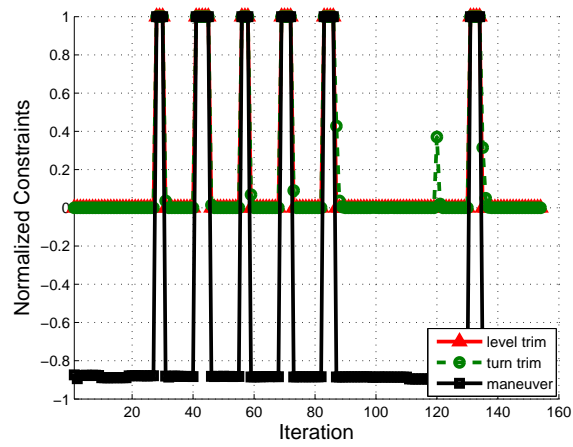


(b) Constraints

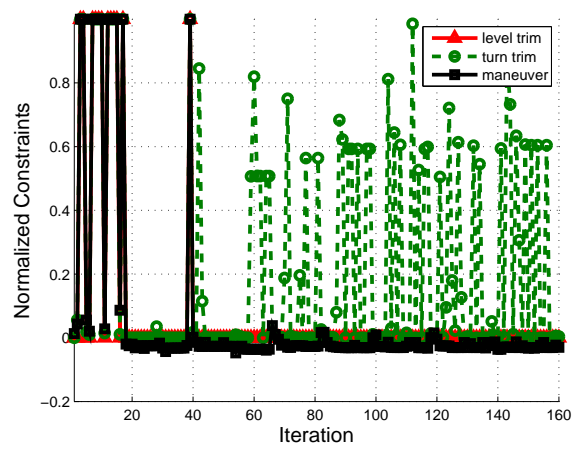


(c) Design variables

Fig. 11. Evolution of objective, constraints, and design variables during the optimization with active constraints.

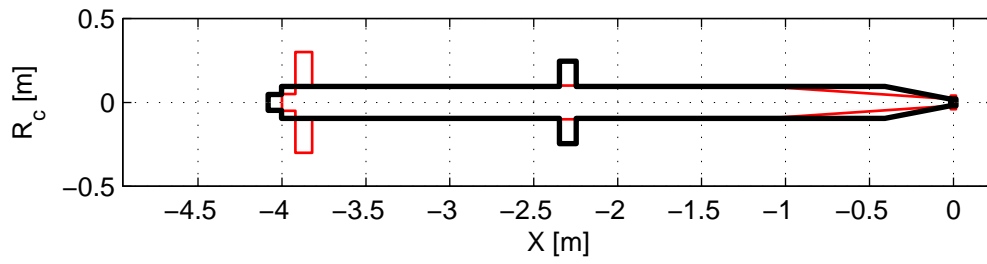


(a) Relaxed constraints

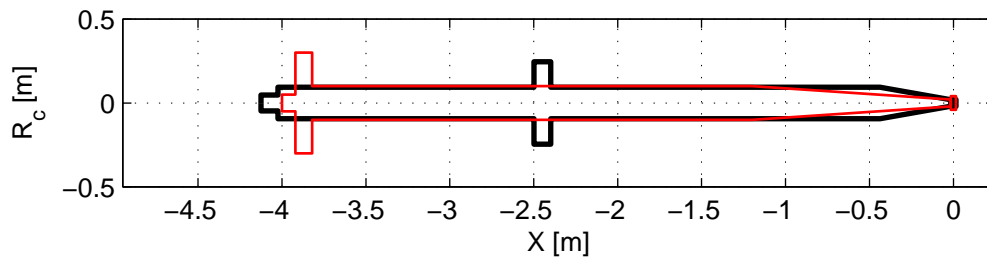


(b) Strict constraints

Fig. 12. Evolution of constraints during the optimization process.



(a) Relaxed constraints:  $n = 1.1$  and  $T_{\max} = 40$  sec



(b) Strict constraints:  $n = 2$  and  $T_{\max} = 4.5$  sec

Fig. 13. Optimal configurations of the supercavitating vehicle obtained through optimization with various constraints.